CrossMark

Analysis of highly directive photoconductive dipole antenna at terahertz frequency for sensing and imaging applications

Isha Malhotra[a], Kumud Ranjan Jha[b], G. Singh[a],*

[a] *Department of Electronics and Communication Engineering, Jaypee University of Information Technology, Solan 173234, India*
[b] *Department of Electronics and Communication Engineering, Shri Mata Vaishno Devi University, Katra, Jammu & Kashmir, India*

ARTICLE INFO

ABSTRACT

In this paper, we have analyzed a photoconductive dipole antenna at terahertz (THz) frequency for sensing and imaging applications. For these applications, to detect powdered explosives, there is a need to have an image of the object under detection with high resolution to distinguish suspicious items from the normal background. The THz antenna is one of the most important components in a THz sensing and imaging system and there is a need to have such a transmitting THz source with high directivity and optimum radiation efficiency. Therefore, to achieve this, we have explored three photoconductive dipole antenna configurations to enhance the directivity and radiation efficiency. With the use of a simple dipole antenna and silicon lens, we are able to achieve the directivity of 10.7 dBi and radiation efficiency of 91.59% in both E-plane and H-plane.

1. Introduction

A portion of the electromagnetic spectrum between the optical and microwave regime which is known as terahertz gap, offers a very innovative sensing and imaging applications [1] and provides the information that is unavailable through the conventional methods such as microwave and X-ray techniques. The terahertz radiations have some unique attractive features such as it can yield extremely high-resolution images in sensing and imaging applications, it is non-ionizing to the molecules in human tissue in biomedical applications and it can move vast amount of data quickly in communication application [2,3]. However, these potential features have been exploited in laboratory demonstrations also to identify explosives [4], reveal hidden weapons [5,6], checking for defects in tiles on the space shuttle [7], screen for skin cancer and tumor [8], and non-destructive testing of composite materials [9–11]. Various proposed applications exploit the unique capabilities of THz radiation to penetrate the packaging materials and therefore provide their spectroscopic information. However, there are certain emerging issues related to THz for imaging and sensing applications [12] such as the water content of the human body prevents transmission-type imaging [13] and the spatial resolution of images with THz radiation is lesser than that with optical light in principle. However, in the real-world scenario, there are nine low-attenuation windows in the range of 0.1–3 THz of the spectrum, (a) 0.1–0.55 THz; (b) 0.56–0.75 THz; (c) 0.76–0.98 THz; (d) 0.99–1.09 THz; (e) 1.21–1.41 THz; (f) 1.42–1.59 THz; (g) 1.92–2.04 THz; (h) 2.05–2.15 THz; and (i) 2.47–2.62 THz, respectively [14]. These

frequency ranges are determined by considering the temperature of the measurements at 23 °C and the relative humidity of 26%. These transmission bands are important to consider because many commonly used solid-state explosives and related compounds (ERCs) have spectral fingerprints in 0.1–2.8 THz range. These fingerprints arise from the intra-molecular and inter-molecular vibrational modes or phonon modes of these explosive materials [15]. Therefore, the THz sensing and imaging in transmission /low attenuation windows is necessary for the detection of the hidden explosives. The THz imaging is based on the use of THz electromagnetic waves to spectroscopically detect and identify concealed explosives like research department explosive (RDX) and high melting explosive (HMX) through their characteristic transmission or reflectivity spectra in the THz range [16].

A detection technique to RDX pellet using THz frequency is as shown in Fig. 1 [4]. In this setup, a femto-second pulsed laser (Ti: Sapphire laser) is used for the generation of signal. The laser beam is splitted into two beams by a splitter, one for exciting photoconductive antenna working as emitter, and the other for measuring the THz signal as ZnTe crystal detector. Various beam splitters are used for the beam deflection. The parabolic optical mirror combination is used for the optical beam to strike the photoconductive material of the emitter to generate the THz beam which is focused on sample point. The sample (RDX pellet) is placed at the THz focus point and perpendicular to the incident beam. The transmitted THz beam is then collected and focused by using the other pair of off-axis parabolic mirrors onto the ZnTe crystal, in which the probe beam detect the THz field by electro-optic sampling. When such radiations are allowed to pass through the

---
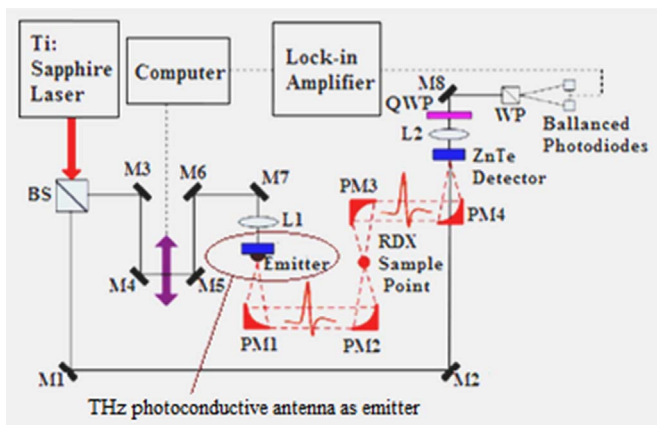
* Corresponding author.

Fig. 1. THz frequency system based on photoconductivity wherein LT-GaAs emitter is used as a THz photoconductive antenna [4].

sample, they get absorbed at their respective features and the absorption coefficients provide the information related to detection of hidden explosives at detector side.

From Fig. 1, it is clear that the photoconductive antenna is one of the most important components in a THz sensing and imaging system as it plays significant role for both impedance matching and power source. In [4], a terahertz time-domain spectroscopy system has been deployed in 0.2–3.4 THz range. The THz bandwidth of a photoconductive antenna is expressed as the range of frequencies over which the measured frequency domain signal strength exceeds the system noise level. However, an increased bandwidth is important for applications that utilize distinct spectral characteristics in materials such as in THz sensing and imaging applications for the detection of hidden powdered explosives and this requires the ability to observe narrow absorption peaks in the THz band. Therefore, increasing the bandwidth of a THz photoconductive antenna based system will allow additional vibrational modes to be quantified [17,18]. Several companies such as TeraView Ltd., Picometrix LLC, Advantest and Menlo Systems offer complete THz imaging and spectroscopy systems which employ photoconductive antennas as emitters and detectors [19]. Some commercially available photoconductive antenna based THz spectroscopy systems by TeraView company with model numbers TPS Spectra 3000 and TeraPulse 4000 have a bandwidth (maximum frequency) of 4 THz and 6 THz, respectively. Similarly, Picometrix and Advantest have developed the spectroscopy systems T-Ray 5000 and TAS each having a bandwidth of 4 THz. The company Mento Systems have developed TERA K8 and TERA K15 spectroscopy systems which are photoconductive antenna based system with a bandwidth of 3.5 THz and 4 THz, respectively.

For the sensing purpose, it is required to have a highly directive low-profile photoconductive antenna which generates the desired THz radiation at operating frequency with high directivity and optimum radiation efficiency with broad bandwidth. However, one of the major problems of the various reported photoconductive dipole antennas is that the antenna efficiency is very low, thus it is difficult to obtain high power THz waves. The photoconductive dipole antenna is unable to convert the laser source power to the THz power efficiently as the best power conversion efficiency reported in literature is much less than 0.1% for pulsed systems [20]. Therefore, the researchers usually increase the illumination power and the applied bias to yield higher output power however in such situations, the phenomena like saturation of charges, velocity overshoot, field breakdown and thermal breakdown occur in the pulsed systems. The thermal and field breakdown must be avoided under any conditions. Furthermore, three main reasons for low efficiency of the photoconductive dipole antennas are: a) space-charge also known as coulomb screening effect and radiation field screening effects, b) spatial non-uniformities, and c) insufficient

acceleration of the charges like inadequate field strength. The coulomb screening effect is due to the space-charge field generated by the photo-excited electron-hole pairs. As the free carrier's movement under the influence of the applied bias field, they generate a static field which partially screens the applied bias field. The radiation screening effect is due to the THz near-field radiation which is also responsible for partially screening the applied bias field. However, the radiation screening effect becomes negligible for typical THz photoconductive dipole antenna in continuous wave operation mode, where the peak optical pulse intensity is high [21]. Further, the spatial non-uniformities occur in photoconductive dipole antenna because the thickness of the substrate is usually larger than the wavelength of THz waves, surface/substrate modes are generated and the antenna performance is sensitive to the substrate. If the thickness of substrate is increased, the dipole antenna couples power to higher-order substrate modes and in some cases, even more than 90% of the power gets trapped in the substrate [22]. Moreover, if a dipole antenna is fabricated on a thick substrate, a surface wave mode can be excited which depends on the frequency, thickness and the relative dielectric constant of the substrate. Therefore, all the power radiated from the dipole structures is not directly transferred into the medium and the fraction of power from the dipole structure is trapped on substrate which also affects the radiation pattern.

In this paper, we have designed a photoconductive THz dipole antenna for the sensing of RDX and HMX whose spectral fingerprints lies in the range of 1–2 THz. This range has been selected because the RDX has the absorption feature band centre position frequency at 1.05 THz, 1.30 THz, 1.50 THz and 1.91 THz and HMX has the absorption feature band centre position frequency at 1.58 THz, 1.84 THz, and 1.91 THz, respectively [4,13]. The remainder of the manuscript is organized as follows. The section II discusses the related work in the field of photoconductive antenna and formulates the research problem. In Section III, the design and estimation of the structure parameters for photoconductive dipole antenna at 1.5 THz frequency has been performed. Section IV covers the detailed description of proposed simulation model. In Section V, the performance analysis of the THz photoconductive dipole antennas based on variation in the aspect ratio of the antenna parameters and analysis of three configurations of THz photoconductive dipole antenna are discussed and finally, Section VI concludes the work.

2. Related work and problem formulation

With context to the microwave sources and detectors, it is difficult to fabricate solid state sources and detectors in THz range because the size becomes very small leading to very small power available [23,24]. In addition to this, the conventional laser sources are also not available at THz frequencies due to unavailability of suitable semiconductor sources. However, with the development of ultra-short pulse femto-second lasers like Ti-Sapphire laser and quantum cascade lasers, it is possible to generate THz signals. The electro-optic rectification (different frequency mixing) method is also used to generate THz radiation but it has certain limitations. This method cannot generate THz frequency signals over broad frequency range and is also very sensitive to optical and thermal noises. Moreover, for the application of sensing and imaging a broadband short-pulse THz source is required in either Time Domain Spectroscopy (TDS) or THz Pulsed Imaging (TPI). Therefore, the photoconductive antenna is one of the simple and stable devices for THz photonics used for sensing and imaging applications at THz frequency. The photoconductive antenna is relatively stable against optical and thermal noises in comparison to the electro-optic rectification [25]. However, the total antenna efficiency which includes optical-laser to THz conversion efficiency, impedance matching efficiency and radiation efficiency is low. Various photoconductive dipole antenna structures are proposed and used for the THz frequency range [26]. On the basis of the architecture of photoconductive antennas for THz pulsed systems, they are classified as

an aperture antennas (large and small compared to wavelength), spiral antennas, bowtie antennas and dipole antennas. In the large aperture photoconductive antenna, the distance between the electrodes is much larger than the centre wavelength of the THz wave and it is range of few hundred micrometers. However, in the small gap photoconductive dipole antenna, the antenna gap distance is only few micrometers. Moreover, in the photoconductive dipole antenna, to increase the conversion efficiency, the electrodes with sharp tip ends can be used and the efficiency can further be improved by putting them in a laterally offset format. In this case, the THz emission can be enhanced with less optical power because of better overlap between the laser spot and high electric field point and also stronger fringing field effects between the electrodes [27]. For small gap photoconductive antennas, the fabrication of such tiny sharp tips is not easy. Moreover, an appropriate configuration of the electrodes may double the efficiency of the antennas, with a consequence in the bandwidth of the radiated pulse. However, the 1st photoconductive antenna was reported by Mourou et al. [28] in the GHz range and then it is extended into the THz region by Auston et al. [29,30]. Grischkowsky et. al. [31,32] has reported the application of optical technique for the generation of diffraction limited THz beams with a relatively large size of the source. This method was further developed at Bell Labs and the IBM Watson Research Centre, and is now used as a commercial product by Picometrix Inc, MI [33]. Moreover, it is important to determine the antenna's spatial response as it is related with the power collected by the antenna. Therefore, the measurements of spatial response of infrared dipole and bow-tie lithographic antennas are discussed by Fumeaux et. al [34]. A dipole antenna situated in a pyramidal horn cavity etched in silicon operated at 0.8 THz is reported in [35]. A stripline dipole antenna for a broad frequency range upto 5 THz on semi-infinite and lens substrates is discussed in terms of input impedance and radiation characteristics in [36].

Further, the emission efficiency of photoconductive dipole antenna is discussed by Tani et al. [13,37], considering the saturation effect due to the field screening by photo-generated carriers. The key features of near-field patterns on the photoconductive antenna are discussed by Hughes et al. [38]. They introduced a finite-difference time-domain method for pulsed-laser-excited vector THz fields from photoconductive antenna. Berry and Jarrahi [39] have evaluated the criteria to optimize the impedance matching in photoconductive antenna. Moreno et al. [40] presented the mobility model to describe the carrier dynamics for the analysis of radiating semiconductor photoconductive devices in the THz regime. The biased electric field analysis of photoconductive antenna for THz generation is reported by Yang et al. [41]. In their simulation results, it is illustrated that the strip-line photoconductive antenna and photo-conductive dipole antenna cannot withstand high biased voltage because of the small value of breakdown electric field of the substrate material. Another exciting new technology for THz antennas is the idea of active surface correction for improving the beam efficiency [42,43]. However, the high directivity with high front-to-back ratio, optimum radiation efficiency, broad bandwidth and tuning or phase scanning is the significant challenges related to the design issues of photoconductive dipole antenna. In this paper, the author's potential contribution to design a photoconductive dipole antenna at THz frequency for sensing and imaging applications are as follows.

- To enhance the directivity of the proposed photoconductive dipole antenna at THz frequency, the structure parameters have been computed and optimized.
- To increase the antenna radiation efficiency which also contributes to the total efficiency of photoconductive dipole antenna, a thin superstrate over the substrate of the dipole antenna is used to enable antenna to withstand high biased voltage.
- For diffraction limited imaging there is a need to design an antenna of shorter wavelength. Accordingly, the proposed antenna design is compact in size and the use of silicon lens helps to focus the beam in the desired direction.

3. Parametric estimation of photoconductive dipole antenna

In this section, three different configurations of THz photoconductive dipole antenna are designed to resonate at 1.5 THz frequency in the presence of 30 V DC bias lines. We are interested to design a THz photoconductive dipole antenna for sensing and imaging to detect the hidden explosives (like RDX and HMX)which shows their spectral fingerprints with absorption peak position in THz regime in the range of 1 THz to 2 THz as reported in [4,14,15]. Therefore, a THz photoconductive antenna is designed at 1.5 THz to detect such explosives easily. Further, one of the main hurdles for THz free-space sensing and imaging is the atmospheric attenuation dominated by the water vapour absorption, however the choice of using 1.5 THz operating frequency is also supported by the transmission windows mentioned in Section I. In addition to this, to analyze the performance of designed THz photoconductive dipole antenna in the frequency range 1 THz to 2 THz is used because many home-made ammonium nitrate bombs and other improvised explosive devices have featureless THz spectra below 3 THz which are posing potential challenges to THz security applications. Therefore, this proposed simple antenna design can also be used for the detection of such explosives having THz spectra below 3 THz. The basic structure of THz photoconductive dipole antenna is shown in Fig. 2, which consists of a dipole antenna structure, a photoconductive substrate and a ground plane placed under the substrate. The antenna has a photoconductive gap (G) at the centre of dipole antenna of effective length (l_e), which is biased with a voltage source (30 V) and is illuminated at the centre with femto-second laser pulse.

By illuminating the photo-conductive layer of the antenna by femto-second laser pulses, the electron-hole pairs are generated when the laser pulse has higher photon energy as compared to that of the band gap energy of the photoconductive material. The applied bias electric field (E_{bias}) across the antenna accelerates these photo-excited carriers. Due to the physical separation of charges, a macroscopic electron-hole field (E_{e-h}) in reverse direction of the bias field is created. With the generation of more electron-hole pairs, E_{e-h} increases and after a while, the total electric field at the position of carriers near the dipole electrodes (defined as $E_{field}=E_{bias}-E_{e-h}$) is screened and described as the reduction in the effective electric field across the antenna gap. By the quick change in E_{field}, the transient current is created and finally, THz pulses are radiated from the photoconductive antenna [44]. The generated transient current decays with a time constant determined by the carrier lifetime in the photoconductive substrate used for the antenna. The radiation efficiency of a photoconductive dipole antenna is proportional to the carrier mobility of photoconductive substrate as presented in [13], but not strongly depends on the carrier lifetime.
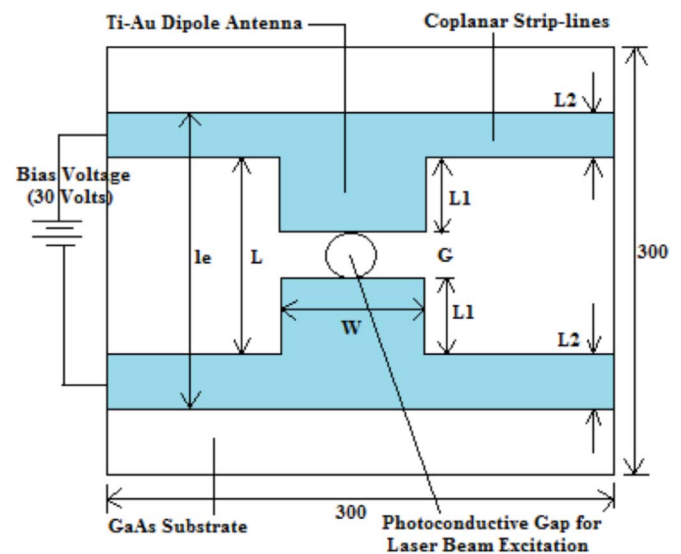

Fig. 2. The basic structure of THz photoconductive dipole antenna.

However, a short carrier lifetime is preferred to reduce the detector noise generated due to the thermal motion of the carrier. Likewise, the antenna efficiency is also proportional to the substrate resistivity because, it increases linearly with the applied biasing voltage. In addition to a low carrier lifetime and high resistivity of photoconductive material, maintenance of relatively high carrier mobility, appropriate band gap, high breakdown voltage and suppression of zero bias photocurrent play an important role and they influence the antenna's output power, maximum optical pump power and bias voltage, bandwidth and signal to noise ratio (SNR), respectively [45–47]. Owing to these properties, gallium arsenide (GaAs), bulk indium gallium arsenide (In GaAs), alternating nanoscale multilayers of InGaAs, indium aluminum arsenide (InAlAs), low-temperature- grown GaAs, radiation damaged silicon on sapphire and amorphous silicon are the most promising substrate materials for THz photoconductive antennas [48]. The proposed antenna in this work usages GaAs substrate which has a photo-carrier lifetime τ_c=0.25 ps, a high mobility 200 cm^2/Vs, a high breakdown field 4×10^5V/cm and has a room temperature bandgap of 1.424 eV (871 nm) [49], making it compatible to the Titanium-doped Sapphire femtosecond pulsed laser sources commonly used to excite photoconductive antennas. If, the thickness of substrate is kept 1 μm then about 30% of the light is absorbed into the substrate and in order to reduce the absorption in substrate below 5%, at least 3 μm of the substrate is required. Therefore, we consider 10 μm thick substrate in this design and its dimension is 300 μm×30 0 μm×10 μm. A lossy-metal Ti-Au is used as the material for the dipole antenna structure placed on the GaAs substrate. Due to the good Ohmic contact between Ti-Au and GaAs, they are used as the antenna and substrate material, respectively. Graphene is also a promising material for the miniaturized resonant THz antennas design [50,51]. However, only few initial works considered the use of graphene in THz antennas. Firstly, graphene was considered as a parasitic layer below a dipole antenna made of gold (Au) and radiated at millimeter wave frequency of 120 GHz [52]. The scattering of an incident wave impinging on graphene rectangular patches was studied in [53] wherein, it was concluded that the graphene patches support surface plasmonic resonances in the THz range. In [54], graphene has been used as an actual antenna radiator where radiation is achieved by placing a THz continuous-wave (CW) photomixer as source in the middle of the graphene patch. The photomixer excites the graphene patches which are DC biased and thus enables its surface to radiate. The 1st physical parameter in the design of photoconductive dipole antenna is the photoconductive gap size (G) where the femto-second laser pulse strikes to generate the photo carriers.

$$E_{THz}^{peak} = e\mu T_{int} \frac{(1-R)}{h\vartheta} \frac{P_{in}}{G} \frac{E_{bias}}{G} \qquad (1)$$

where, e, μ, T_{int} R, $h\vartheta$, P_{in}, G, and E_{bias} are electron charge, carrier mobility, pulse interval, reflection from the photoconductive substrate, photon energy, average pump laser power, photoconductive dipole antenna gap size and bias voltage, respectively. From Eq. (1), it is clear that the emission efficiency is inversely proportional to the photoconductive dipole antenna gap when the bias field (E_{bias}) and pump-power (P_{in}) are constant. Therefore, it is important to use a photoconductive gap as small as possible by focusing the laser beam (optical excitation) very closely to the gap. This is also true when the pump laser power is low, the efficiency saturates at higher pump intensities. Moreover, the antenna gap needs to adjust such as to alleviate the screening effect (the cancellation of a portion of the bias field by the transient current at the surface when the near field is generated) and as a result improve the efficiency in THz photoconductive dipole antenna which influences the initial spatial distribution of photo-excited carriers on photoconductive substrate. The photoconductive gap is taken as 5 μm for small gap photoconductive dipole antenna in all three antenna designed configurations and its value is optimized using the simulation software (CST Microwave Studio). The length of coplanar strip-line is usually set to be long enough to avoid the reflection at the line end. Therefore, the length of coplanar strip-line taken is 300 *μm*, width 10 μm and thickness 0.35 *μm*. The length of the dipole is determined using the relation of resonant frequency as f_r=c/2nL, where c, L, and n are the speed of light in vacuum,

separation between two coplanar strip-lines and refractive index of the material, respectively. For the resonance, $L = m \times \lambda_n/2$, where m=1,2,3...., and the wavelength λ_n in the material depends on the refractive index n which is given by $\lambda_n = \lambda/n$. If we take m =1, then $L = \lambda/2n$. The refractive index of the semiconductor material for GaAs at THz frequencies is 3.4 and for f=1.5 THz, the value of L (length of dipole) is: L= C/(2nf_r) =30 μm. The other equally important physical parameter of the photoconductive dipole antenna is the width (W) of dipole because of two reasons: 1) the directivity and 2) radiation efficiency of the photoconductive dipole antenna which strongly depends on the relative dimensions of the dipole as both increases significantly by increasing the aspect ratios ($\eta \equiv L/W$). The emission efficiency can also be increased by increasing the aspect ratio (L/W) of the THz photoconductive dipole antenna as reported in [55]. However, an optimum value of aspect ratio for photoconductive dipole antenna can be determined by considering the following factors:

- The emission intensity significantly decreases as the dipole length decreases.
- With increase in the dipole length, the peak frequency of emission spectra shifts to lower frequency.
- The bandwidth becomes narrower as the dipole length increases.
- The peak intensity decreases significantly with increase in the dipole width, which reveals that the emission efficiency of dipole antenna is proportional to the aspect ratio.

From the aforementioned points, it is concluded that for the better performance of THz photoconductive dipole antenna, the length of dipole must be greater than the width of dipole. In the proposed antenna, we have also checked the performance of the antenna with different values of the aspect ratio by keeping the length of dipole constant to 30 μm and varying the width of the dipole to set the aspect ratios as (L/W) 0.5, 1,1.5,2, with the values of width of dipole (W) as 60, 30, 20, 15 (all in μm), respectively. It is observed from the simulated results discussed in section V, that by keeping aspect ratio 1.5, the performance of THz photoconductive dipole antenna is interesting in terms of directivity in both the E- and H-planes. Further, the other physical parameter of photoconductive dipole antenna is the effective length (l_e) and its value has been computed considering following points.

- If the effective length of dipole is assumed to be same as the distance between coplanar strip lines i.e. $l_e = L$, then in this case l_e =30 μm
- If the effective length of the dipole antenna is taken into the account: $l_e = 2L_2 + L$, and in this case l_e =50 μm with L_2, the width of the strip-line which is 10 μm.

The choice of considering the effective length will affect the resonating frequency as f_r = c/(2l_e[(1+ε_d)/2]$^{1/2}$), where f_r and $\in_d$ are the resonating frequency and the dielectric permittivity of GaAs substrate, respectively. If the effective length of dipole is assumed to be the same as the distance between the coplanar strip-lines i.e. $l_e = L$, then by using c =3×10^8 m/s, l_e=30 μm and ε_d=12.9 for GaAs, the resonance frequency f_r =1.89 THz. If the effective length of dipole antenna is chosen by considering the width of coplanar strip-lines i.e. l_e=2$L_2 + L$, then the resonance frequency is f_r =1.14THz. Now, by considering the values of physical parameters determined for the THz photoconductive dipole antenna of Ti-Au (lossy-metal) material with conductivity σ=1.6× 10^7 S/m and thickness 0.35 μm, is designed on a photoconductive substrate GaAs (lossy) having dielectric permittivity ε =12.94, magnetic permeability μ =1 and loss tangent δ=0.006 S/m. The antenna designed with this specifications is named as Design-A in the manuscript. However, we are interested to use this THz photoconductive dipole antenna for sensing and imaging application wherein high directivity is required, therefore for this purpose, two more designs are simulated. The Design-B is configured by using a superstrate which helps to enhance the radiation performance and efficiency of THz photoconductive dipole antenna [56]. A very thin superstrate of low-temperature grown GaAs (LT-GaAs) with thickness 1 μm is placed in

between the GaAs substrate and the antenna structure. In other antenna configuration that is Design-C, a silicon lens is used to enhance the directivity of the THz photoconductive dipole antenna. A small hemispherical Silicon lens is placed beneath the ground plane which is the direction of propagation of generated THz wave from the photoconductive dipole antenna. The potential importance of using thin LT-GaAs superstrate and a silicon lens in the THz photoconductive dipole antenna is discussed as follows.

• *Use of thin LT-GaAs Superstrate*

When the photoconductor is illuminated by a short optical pulse, a current surge as shown in Fig. 3 is noticed which leads to THz radiation. If the carrier lifetime is long then the current keeps flowing long after the excitation pulse is disappeared. This has the effect of broadening the photocurrent pulse, which results into broaden the output pulse and reduce the overall THz frequency bandwidth. If, another pulse arrives before the current dies out and excites the photoconductive dipole antenna, a new THz pulse is generated, but at this time the background current which is already present may affect the THz generation. Therefore, to prevent this, photoconductors with subpicosecond carrier lifetime such as low-temperature-grown gallium arsenide (LT-GaAs) having very small thickness in comparison to the GaAs substrate, may be used.

Moreover, the THz photoconductive dipole antenna with a thin layer (nearly 1 μm) of short carrier lifetime LT-GaAs as superstrate can avoid saturation at high frequency which helps to achieve peak power spectral density. The LT-GaAs has the relevant features such as very high electric breakdown field (~ 500 kV/cm), short photo-carrier lifetime (0.1 ps) along with high mobility of charges (> 200 cm^2/Vs), therefore it is a good material for fabrication as a superstrate in the photoconductive antenna.

• *Use of Silicon Hemispherical Lens*

Due to the ease of built-up, the extended hemispherical dielectric lens (Silicon lens) is used to increase the directivity of an antenna. The Silicon lens reduces loss because of reflection and refraction of radiation at the substrate-air interface [57] and such a lens that is a hemisphere of radius R, is located directly on the ground plane of THz photoconductive dipole antenna. The directivity D of a lens antenna in the direction of the main lobe can be found from the formula for the

directivity of a circular aperture with the radius R and uniform distribution of the electric field [58], as $D = 20\log ((2\pi R)/\lambda_0)$, where λ_0 is the wavelength in free-space and R is the lens radius. The width of the beam at −3 dB of the directivity of the integrated lens antenna can be estimated as $\Omega = 59°(\lambda_0/2R)$. The use of a lens with THz photoconductive dipole antenna also provides the electronic beam-steering capability to the antenna by switching between two photo-conductive dipole antenna elements with common bias lines and the ground plane. In such a case, the photoconductive dipole antennas need to be placed on a plane focal surface of the lens. The electronic beam steering allows antenna to automatically adjust the beam direction during initial alignment of transmitting and receiving antennas [59] and thus the photoconductive dipole antenna array with lens may be used for THz pulsed imaging with scanning.

4. Simulation model

In the small gap photoconductive dipole antenna, the gap is of only few micrometers (μm) and thus, there is an insufficient acceleration of the charges which results in the inadequate field strength to generate THz radiations in comparison to that of the large aperture photo-conductive antenna which results low antenna efficiency. Therefore, to increase the radiation efficiency of photoconductive dipole antenna, it is important to consider the factors which affects the total antenna efficiency. In the photoconductive dipole antenna, three types of efficiencies are considered to evaluate the total antenna efficiency (η_t), which are 1) laser-to-electrical conversion efficiency (η_{LE}), 2) impe-dance matching efficiency (η_m) and 3) radiation efficiency (η_r). The total efficiency of photoconductive dipole antenna also known as optical-to-THz power conversion efficiency, which is the multiplication of these three efficiencies, is:

$$\eta_t = \eta_{LE} \times \eta_m \times \eta_r \tag{2}$$

• *Computation of laser-to-electrical conversion efficiency*

When the optical pulse is incident on the photoconductive gap of the proposed antenna, the induced photocurrent is expressed as [60]:

$$I = \frac{eE_{bias}\mu_e\tau\eta_L P_L}{hf_L G^2} \tag{3}$$

where e, E_{bias}, μ_e, τ, h, G, f_L, P_L, and η_L are electron charge, the applied bias voltage, free-carrier mobility of the photoconductor, photocurrent decay time, Planck's constant, gap length, laser fre-quency, laser power incident on the gap, and the illumination efficiency, respectively. The illumination efficiency takes into account of many issues such as the reflection of laser on the surface of substrate and quantum efficiency. The laser is focused on the feeding gap and the photon energy of the laser is equal to or slightly greater than that of the band gap of the semiconductor substrate to ensure that free-electrons are efficiently generated. This electro–optical operation converts the laser power P_L to electrical power P_E. To obtain the electrical power, first, it is important to obtain the associated resistance, R such as:

$$R \approx \frac{hcf_R g^2}{\eta_L e\mu_e P_L \lambda_L} \tag{4}$$

where f_R is the laser repletion frequency. From Eqs. (3) and (4), the induced electric power on the photoconductor is:

$$P_E = I^2R \approx \left(\frac{eE_{bias}\mu_e\tau\eta_L P_L}{hf_L g^2}\right)^2 \frac{hcf_R g^2}{\eta_L e\mu_e P_L \lambda_L} \tag{5}$$

Therefore, from Eq. (6), the laser-to-electrical power conversion efficiency is estimated as:
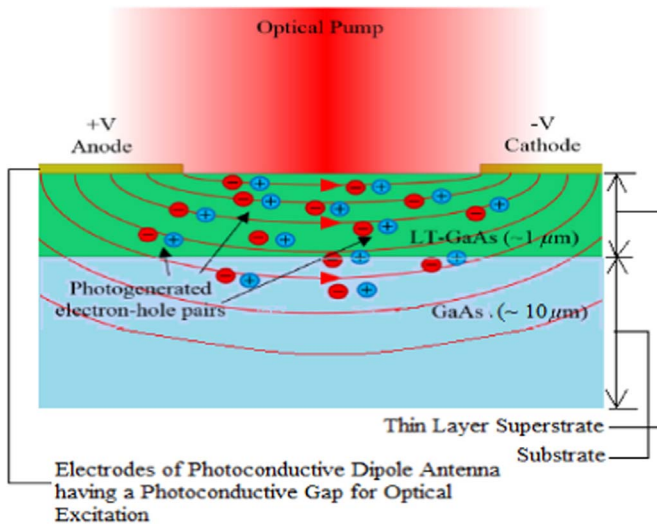

Fig. 3. Optical carrier generation at the photoconductive dipole gap of a LT-GaAs superstrate based THz photoconductive dipole antenna and the red arrows represent the flux lines of the electric field [19]. (For interpretation of the references to color in this figure legend, the reader is referred to the web version of this article.)

$$\eta_{LE} = \frac{P_E}{P_L} \approx \frac{eE_{bias}{}^2\mu_e\tau^2\eta_{LI}f_R}{hf_L g^2} \qquad (6)$$

From the Eq. (6), it is clear that in addition to the laser source, this efficiency factor has included another source which is the bias voltage and thus, the electric power is not solely provided by the laser source.

- *Calculation of impedance matching efficiency*

The impedance matching efficiency is:

$$\eta_m = 1 - \left(\frac{Z_a - Z_s}{Z_a + Z_s}\right)^2 \qquad (7)$$

where Z_a and Z_s are the antenna impedance and source impedance, respectively. The value of source impedance is determined from the time-varying source conductance. The time-varying source conductance in the THz photoconductive dipole antenna depends on the values of length and width of the gap. The time-variant resistance of photoconductive material is the inverse of $G_S(t)$ and this can be used to compute the time (frequency) variant impedance matching efficiency of the THz photoconductive dipole antenna. The time-varying source conductance $G_S(t)$ is:

$$G_S(t) = \frac{W}{G}e\mu_e I_l\tau_l(1-R)\frac{\sqrt{(2\pi)}}{4h\upsilon}[1-\exp(-\alpha T_{LT-GaAs})]\left[\exp\left(\frac{-2r^2}{w_0^2}\right)\right]$$
$$\left[\exp\left(\frac{\tau_l^2}{8\tau_c^2} - \frac{t}{\tau_c}\right)\right]\left[\mathrm{erf}\left(\frac{\sqrt{2}}{\tau_l}t - \frac{\sqrt{2}}{4\tau_c}\tau_l\right)+1\right] \qquad (8)$$

where α, $T_{LT-GaAs}$, μ_e, I_l, R, τ_l, and τ_c are the optical absorption coefficient, thickness of the substrate, electron mobility, peak laser intensity, reflection coefficient for the substrate material, laser pulse duration and, the carrier lifetime or trapping time of substrate, respectively.

- *Computation of Radiation Efficiency*

The radiation efficiency of photoconductive dipole antenna is the ratio of gain and directivity of the antenna at the chosen frequency of operation, which is obtained using an electromagnetic simulation tool CST Microwave Studio. However, the low radiation efficiency is the major challenge to the present photoconductive dipole antenna and it occurs due to the excessive Ohmic losses at THz frequencies. In addition, the impedance matching efficiency of antenna must be taken in account for proper impedance matching of laser source with photoconductive material of antenna. It is necessary to mention here that the THz photoconductive dipole antenna is simulated by using the CST Microwave Studio. It provides a simulation platform for all kind of electromagnetic field applications. We have used the Transient Solver which is based on the Finite Integration Technique (FIT), and applies direct time-domain analysis and broadband computation of S-parameters from one single calculation run by applying DFTs to time signals. This simulation run is also supported by the adaptive mesh refinement in 3D using S-parameters supported by the Transient solver of CST Microwave Studio. The structure parameters considered for the proposed antenna is presented in Table 1.

In the photoconductive antenna, the optical source is a femtosecond laser pulse which has a Gaussian distribution at its output, therefore in the CST MSW simulation software, we have applied the Gaussian beam excitation into the substrate from the gap of photoconductive dipole antenna. The antenna configurations which are designed in CST Microwave studio are shown in Fig. 4.

In the present work, we have determined the length (and effective lengths) of the photoconductive dipole antenna for a specific terahertz frequency and the corresponding resonant frequencies have been computed numerically. We have used the CST Microwave Studio to obtain the S_{11} parameter from which, the resonant peaks can be

Table 1
The structure parameters for the proposed antenna.

Parameter	Value
Dipole Antenna (Ti-Au) and Ground Conductivity (S/m)	1.6×10^7
Superstrate(LT-GaAs)	
Carrier Lifetime, majority carriers (psec)	0.1
Mobility (cm^2/Vs)	Greater than 200
Dielectric Permittivity	13.26 [34]
Magnetic Permeability	1
Loss tangent (S/m)	0.006
Electric breakdown field (V/cm)	Greater than 5×10^5
Substrate (GaAs)	
Carrier lifetime, majority carriers (psec)	0.25
Mobility (cm^2/Vs)	200
Dielectric permittivity	12.9
Magnetic permeability	1
Loss tangent(S/m)	0.006
Electric breakdown field (V/cm)	Nearly 4×10^5
Silicon lens	
Permittivity	11.9
Permeability	1
Loss tangent (S/m)	0.00025
Voltage Source	
DC voltage (V)	30

determined and is compared with the values of resonant frequencies obtained mathematically. If we refer Fig. 6 "The S-parameter (dB) for three proposed antenna design configurations" the three resonant peaks obtained for each antenna design are nearly same as that of the theoretical obtained values. However, a multi-physics finite-element solver (COMSOL) may be used to estimate the response of the photoconductor with the designed dipole to an incident optical pump. For this purpose, the photo-generated carrier density may be derived from the calculated optical intensity in the photo-absorbing substrate and combined with the bias electric field data in the classical drift-diffusion model to calculate the induced photocurrent [39]. The incident optical pump from a laser such as Ti: sapphire laser with a central wavelength of 800 nm, 76 MHz repetition rate, and 100 $f$sec., pulse width can be tightly focused onto the photoconductive antenna gap and positioned near the anode contact electrode to maximize the radiated power [61]. The generated terahertz power from photoconductive emitter can be measured using a pyroelectric detector. Moreover, to determine the photoconductive dipole emitter characterization in terms of device alignment, output power measurement and radiation spectral characterization, the steps which are required experimentally, are briefed as follows:

Step 1: Device alignment.

a. Place the aluminium washer carrying the photoconductive terahertz emitter and tightly focus the optical pump from a Ti: Sapphire mode-locked laser (such as MIRA 900D V10 XW OPT 110 V) onto the active area i.e. the photoconductive gap between the dipole electrodes.

b. Use the parametric analyser to simultaneously apply bias voltages to co-planar striplines/ transmission lines of photoconductive dipole antenna and measure the induced electric current. To confirm the optimum optical pump alignments and polarization adjustment by maximizing the photocurrent of device under test.

Step 2: Output power measurement.

a. Use an optical chopper (such as Thorlabs MC2000) to modulate the optical pump from the mode-locked pump laser incident on photoconductive dipole antenna gap.
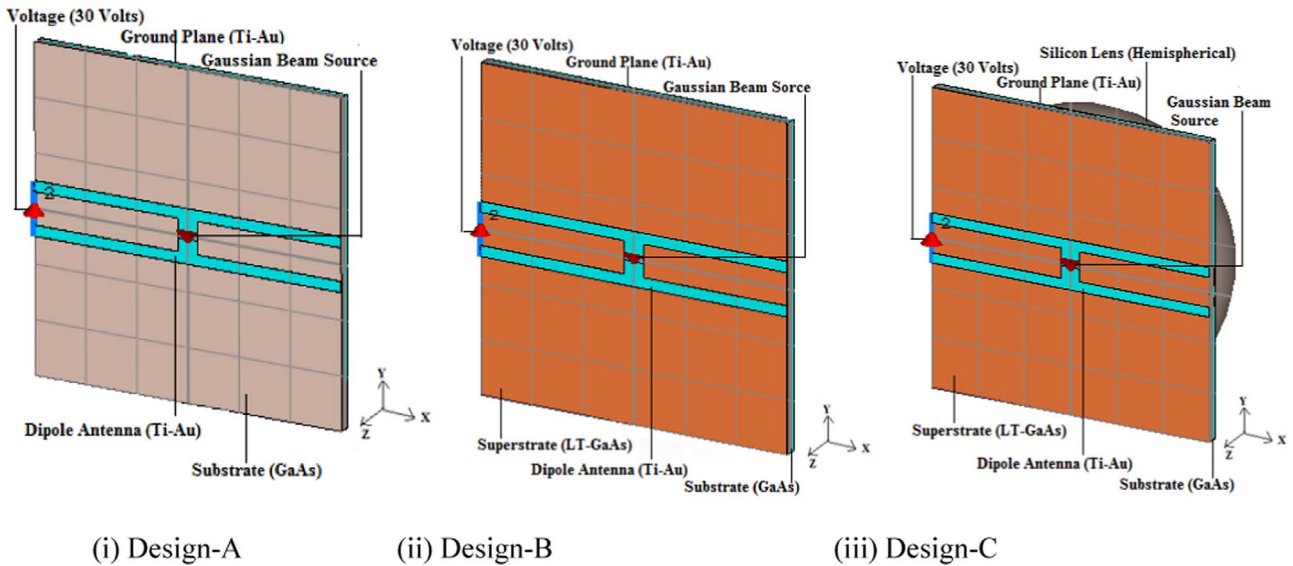
Fig. 4. Three configurations i) Design-A: Basic THz photoconductive dipole antenna, ii) Design-B: THz photoconductive dipole antenna with LT-GaAs superstrate, and iii) Design-C: THz photoconductive dipole antenna with LT-GaAs superstrate and silicon lens.

b. Measure the output power of the photoconductive terahertz emitter using a pyroelectric detector (such as Spectrum Detector, Inc. SPI-A-65 THz).

c. Connect the output of the pyroelectric detector to a lock-in amplifier (such as Stanford Research Systems SR830) with the optical chopper's reference frequency to recover terahertz power data at low noise levels.

Step 3: Radiation spectral characterization.

a. Start with a Ti:Sapphire mode-locked laser and use a beam splitter to split the output of the mode-locked laser into a pump beam and a probe beam.

b. Use an electrooptic modulator (such as Thorlabs EO-AM-NR-C2) to modulate the optical beam in the pump path. Focus the pump beam onto the active area of the photoconductive emitter under test to generate terahertz radiation.

c. Collimate the generated terahertz beam using a first polyethylene spherical lens. Focus the collimated terahertz beam using a second polyethylene spherical lens.

d. Before the focusing the terahertz beam, merge the collimated terahertz beam with the probe optical beam using an ITO coated glass filter.

e. Place a 1 mm thick, < 110 > ZnTe crystal mounted on a stage at the combined focus of the optical and terahertz beam.

f. Insert a controllable optical delay line in the optical probe path by using a motorized linear stage (such as Thorlabs NRT100) to vary the time delay between the optical and the terahertz pulses interacting inside the ZnTe crystal.

g. Split the optical beam into two branches by a Wollaston prism. Then measure the optical beam power in each branch with the help of two balanced detectors connected to a lock-in amplifier.

h. Connect the motorized delay line and lock-in amplifier to a computer wherein a Matlab script is written to iteratively move the position of the motorized delay line, the pause, and read the signal magnitude from the lock-in amplifier.

i. Convert the stage position to the time domain by dividing the total optical delay length by the speed of light which is to be followed by a discreet Fourier transform (using Matlab) to obtain the frequency domain data.

5. Simulation results and discussions

Initially, the comparison of THz photoconductive dipole antenna (Design-A) with different aspect ratio (L/W) is performed, choose and optimize the L/W for the proposed reference antenna (Basic THz photoconductive dipole antenna). The length and width of the co-planar strip lines is assumed constant 300 μm and 10 μm, respectively. The thickness of substrate and ground plane is 10 μm and 0.35 μm, respectively with the antenna thickness 0.35 μm. The distance between striplines (L) is kept constant 30 μm and the width of the gap W is varied to observe the effect of aspect ratio on the performance of THz photoconductive dipole antenna. The values of W are choosen as 60, 30, 20, 15 (all in μm), respectively with fixed L as 30 μm. The comparison for several aspect ratios in terms of gain and directivity is presented in Table 2.

The antenna efficiency is another important parameter which needs to be enhanced to use the antenna in the sensing and imaging applications. Therefore, for different aspect ratios, the radiation efficiency of the basic THz photoconductive dipole antenna is also presented in the Fig. 5.

From Table 2 and Fig. 5 it is observed that the selection of aspect ratio is chosen either L/W=1 or L/W =1.5. If we choose the aspect ratio less than 1 then the gain and directivity of Design-A are interesting with respect to simple dipole design but the radiation efficiency is too small. On the other hand, if we choose the aspect ratio 2, the gain reduces. Furthermore, we have chosen the aspect ratio as 1.5 and for this L and W are 30 μm and 20 μm, respectively. Further for this selection when the sufficient power is provided by the laser to pump the

Table 2
Comparison of gains and directivity in both E and H plane photoconductive dipole antenna for several aspect ratio.

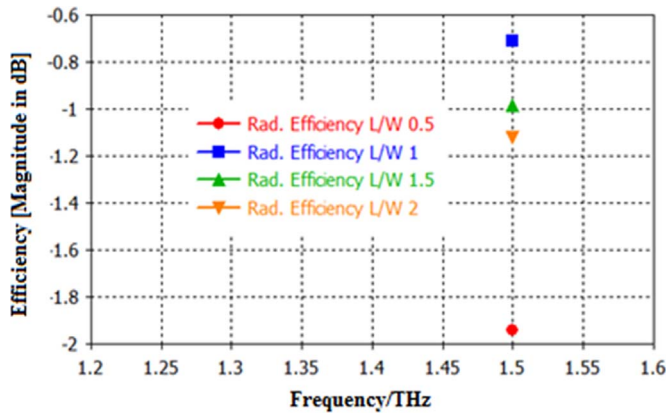| Aspect ratio (L/W) of THz photoconductive dipole antenna	Co-polar Gain (dB) E-plane	Co-polar Gain (dB) H-plane	Directivity (dBi) E-plane	Directivity (dBi) H-plane
0.5	3.24	8	5.18	9.94
1.0	3.31	9.03	4.02	9.74
1.5	3.13	8.71	4.11	9.69
2.0	3.06	8.59	4.17	9.71

Fig. 5. Radiation efficiency at different values of aspect ratio of Design-A(THz photoconductive dipole antenna).
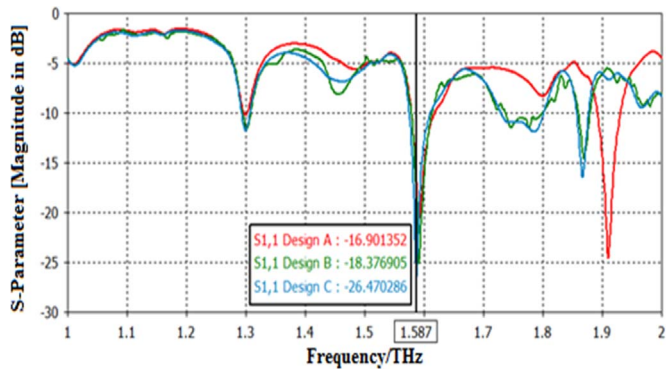

Fig. 6. The S-parameter (dB) for three proposed antenna design configurations.

overall photoconductive gap, then the peak intensity decreases significantly with increase of the dipole width that result constant total input current. Therefore, the width of dipole must be smaller than the length of the dipole. With the aspect ratio 1.5, the dipole length 30 μm and width of dipole 20 μm are considered for the design of basic photoconductive dipole antenna Design-*A*. The S-parameter (in dB) for: 1) Design-A, 2) Design-B and 3) Design-C are compared for the S-parameter (in dB) as shown in Fig. 6. The resonant peaks observed in the results are in accordance with the expressions of resonance frequency discussed in section III with small deviations from their theoretical values. For all the three designed configurations, three

bands are observed below −10 dB as shown in Fig. 6, and the comparison is performed corresponding to the highest resonant peak at f =1.587 THz.

In Design-A, the S_{11} parameter at 1.3 THz, 1.593 THz and 1.9 THz are -10.22 dB, −20.32 dB and −24.568 dB, respectively. The 10 dB impedance bandwidths obtained for each centre frequency are 50 GHz, 39 GHz and 39 GHz, respectively. For Design-B, the S_{11} parameter at frequencies 1.301 THz, 1.587 THz and 1.868 THz are −11.65 dB, −18.37 dB and −16.30 dB, respectively. The 10 dB impedance bandwidths obtained for each centre frequency are 14 GHz, 36 GHz and 20 GHz, respectively. Similarly, for the Design-C, the return loss values at frequencies 1.301 THz, 1.587 THz and 1.868 THz are 11.55 dB, 26.47 dB and 14.09 dB, respectively and the 10 dB impedance bandwidths are 13 GHz, 35 GHz and 20 GHz, respectively. The potential reasons for small deviation in resonant peaks are: a)The resonance phenomena will appear when the quality (Q) factor of the antenna is large enough. However, the THz field does not propagate (and reflect) for a large distance along the antenna due to the strong loss (like radiation loss and dielectric loss). Subsequently, the Q-factor of the THz antenna is small (no standing wave) and thus the resonance effect is not effective as that in the microwave frequencies, b) another reason is the slow decay time of photocurrent (0.5 ps) limiting the generation of higher-frequency components of radiation and c) the absence of resonance peaks at expected frequencies should be attributed to other factors also, such as the broadening of the resonance peak as a result of the large antenna width or the damping of the switching response because of the capacitance of photoconductive gap at high frequency. The performance of proposed antenna designs (Design-A, Design-B and Design-C) are also compared for Gain (dB) and Directivity (dBi), in the principal plane patterns. The simulated results are shown in Figs. 7 and 8.

For Design-A, the gain is 3.13 dB in E-plane with main lobe direction at 0°. The angular width (3-dB) is 34.2° and the side lobe level is −0.8 dB and in H-plane, the gain is 8.71 dB with its main lobe direction is 40.0°. The angular width (3-dB) is 18.2° having a side lobe level −5.6 dB. The directivity at E-plane is 4.11 dBi with main lobe direction at 0°.

The angular width (3-dB) is 34.2° and the side lobe level is −0.8 dB, and for H-plane, the directivity is 9.69 dBi with its main lobe direction is 40°. The angular width (3-dB) is 18.2° having a side lobe level −5.6 dB. The radiation efficiency obtained in E-plane and H-plane are 0.76 and 0.89 with power flow 5.12× 10^{10} VA/m^2. As the radiation efficiency in E-plane is less than 80% and to increase the radiation efficiency of the THz photoconductive dipole antenna, a thin superstrate is used in this reference design.
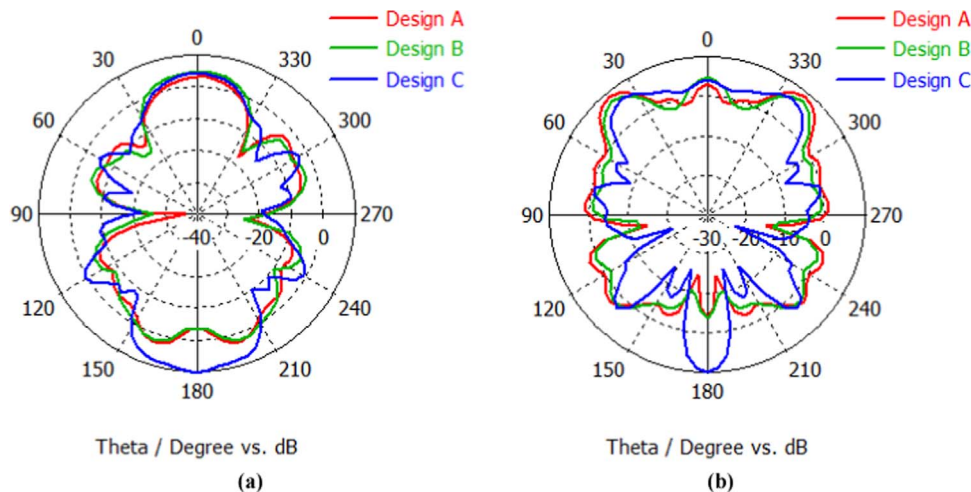

Fig. 7. The antenna gain characteristics of all three configurations in (a) E-plane, (b) H-plane.
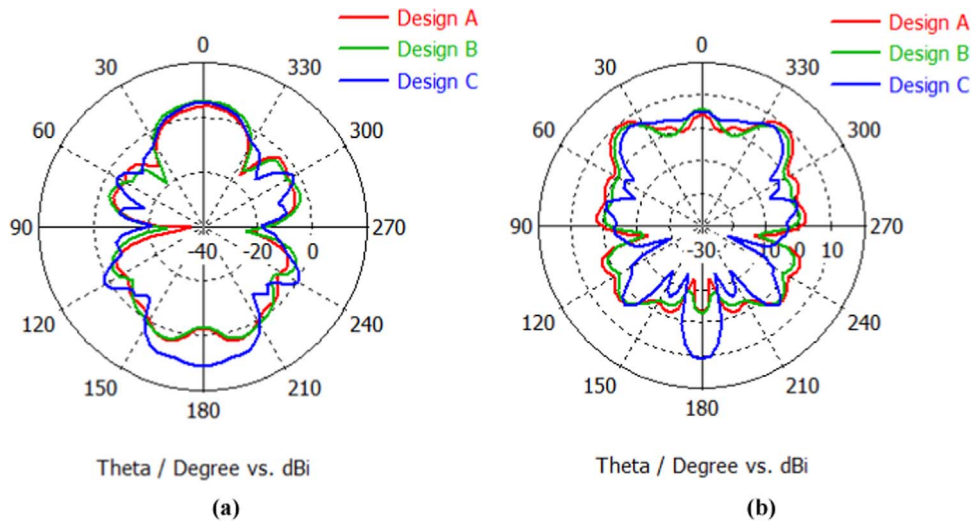
Fig. 8. The antenna directivity of all three configurations in (a) E-plane, (b) H-plane.

The simulated results for Design-B show the gain of 4.85 dBi in E-plane with main lobe direction at 0°. The angular width (3-dB) is 39.6° and the side lobe level is −3.0 dB. However, for H-plane, the gain is 7.3 dBi with its main lobe direction 40°. The angular width (3-dB) is 18.5° having a side lobe level −2.5 dB. The directivity in E-plane is 5.78 dBi with main lobe direction at 0°. The angular width (3-dB) is 39.6° and the side lobe level is −3.0 dB and for H-plane, the directivity is 8.24 dBi with its main lobe direction 40°. The angular width (3-dB) is 18.5° having a side lobe level −2.5 dB. The radiation efficiency obtained in E-plane and H-plane are 0.84 and 0.89 with power flow 6.24×10^{10} VA/m^2. It is clearly observed from the simulated results that the radiation efficiency has been increased in the E-plane from 76% to 84% along with the increase in the directivity from the 3.13 dBi to 5.78 dBi for the same direction of main-lobe i.e. 0°. Moreover, other interesting point which has been observed is that with the use of thin superstrate (LT-GaAs) along with the substrate (GaAs), the power flow has also been increased.

For the purpose of THz sensing applications there is a need of high-directional scanning photoconductive antennas with inexpensive steer-able integrated lens. As the proposed photoconductive dipole antenna is a simple configuration, thus, it allows to use the focusing properties of the lens to excite directed radiation. Therefore, to increase the directivity of THz photoconductive dipole antenna, we have used a silicon lens placed beneath the ground plane that is Design-C from where the THz radiations are generated. The simulation results for Design-C show the value of gain 9.8 dBi in E-plane with main lobe direction at 180.0°. The angular width (3-dB) is 42.8° and the side lobe level is −5.5 dB. For the H-plane, the gain remains same which is 9.8 dBi with its main lobe direction same as in E- plane i.e. 180°. The angular width (3-dB) is 13.4° having a side lobe level −3.5 dB. The directivity in the E- and H-planes is also having same values 10.7 dBi with main lobe direction at 180° for both cases. The angular width (3-dB) is 42.8° in the E-plane and the side lobe level is −5.5 dB. However, for H-plane, the directivity has the angular width (3-dB) as 13.4° having a side lobe level −3.5 dB. The radiation efficiency obtained in E- and H-planes are 91.59% with power flow 5.93×10^{10} VA/m^2. It is clearly observed from the results that the radiation efficiency has been increased and is uniform in both the E-and H-planes. Therefore, the use of Silicon lens helps to enhance the gain and directivity values uniformity in both the principle planes. Moreover, according to the dipole approximation, the radiated electric field from a point source is proportional to the time derivative of the point current in far-field and with a simple extension to this principle, the electric field from a distributed current is achieved by the volume integration of the time-derivative of the current density, J(r′,t′) which is defined at a point, r′

and time t′ [29]. The THz electric field emitted from a photoconductive antenna is expressed as:

$$E_{THz}(r,\ t) = -\frac{1}{4\pi\varepsilon c^2} \int_0^{l_e} \left[\frac{\partial J(r',t')}{\partial t'} \right] \frac{\sin}{|r-r'|} d^3x' \tag{9}$$

where $E_{THz}(r, t)$ is the THz electric field at the observation point, r, and the observation time, t. ε is the dielectric constant of the medium, $J(r',t')$ is the photoconductive current density on the photoconductive dipole antenna. Θ is the angle between the current direction and observation direction. When a constant bias field, E_{bias}, is applied to the photoconductive gap, the current density J(r′,t′) in the photoconductive gap is given by:

$$J_{PC}(t) = \frac{\sigma(t)E_{bias}}{\left[\frac{\sigma(t)Z_0}{1+n}+1 \right]} \tag{10}$$

where $\sigma(t)$ is the conductivity of the photoconductive material. Z_0 is the characteristic impedance of the free-space and n is the refractive index of the substrate. The numerator of Eq. (10) corresponds to the ordinary Ohm law and denominator corresponds to the saturation effect due to the field screening by the charged carriers. With the simulation, we have also illustrated the current density distribution of each of proposed antenna configurations (Design-A, Design-B and Design-C) as shown in Fig. 9.

In the Design-A, a very high current density 4×10^5 A/m is observed because the use of thick photoconductive substrate (GaAs) with thickness 10 μm. For the Design-B and Design-C, the value of current density is 1.38×10^5 A/m and 1.42×10^5 A/m, respectively. The lower values of current density are due to the use of thin layer of superstrate LT-GaAs placed over the GaAs substrate. It is also observed from the Fig. 8 that in the Design-C, the current density is more at the centre of the substrate near the photoconductive gap in comparison of the sides of substrate. This may be due to the use of Silicon lens which is making the THz field highly directive in both the principle planes patterns in the main lobe direction at 180°.

6. Conclusion and future scope

In this paper, we have presented a simple synthesis technique to determine the physical parameters of photoconductive dipole antenna, which is used for THz sensing and imaging applications. For the Design-A, the choice of simple dipole antenna with small gap geometry has been proposed because of its simplicity in fabrication. However, the basic photoconductive dipole antenna illustrates low values of directivity and radiation efficiency. Therefore, by using thin superstrate (LT-
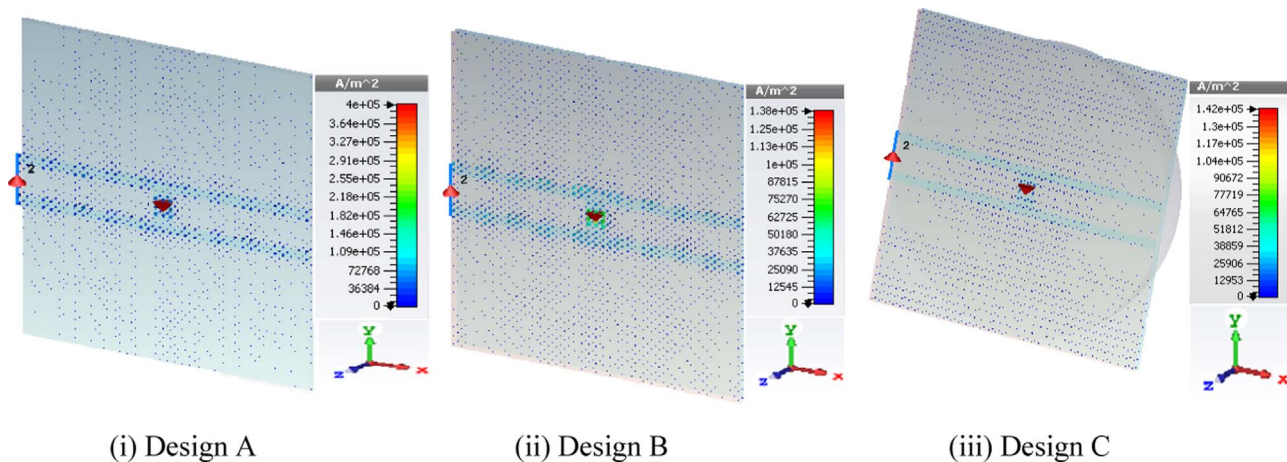
Fig. 9. The current density distribution on the planar surface of three configurations presented using CST Microwave Studio, (i) Design-A: Basic THz photoconductive dipole antenna, (ii) Design-B: THz photoconductive dipole antenna with LT-GaAs superstrate, and (iii) Design-C: THz photoconductive dipole antenna with LT-GaAs superstrate and silicon lens.

GaAs) in the Design-B, the radiation efficiency increases in the E-plane from 76% to 84% along with the increase in directivity from 3.13 dBi to 5.78 dBi. Further, the proposed basic geometry of photoconductive dipole antenna with silicon lens is presented which enhances the antenna performance that is potentially useful for THz sensing and imaging application like the detection of hidden explosives (RDX, HMX, PETN, and TNT) along with some commonly used explosive related compounds. This proposed antenna (Design-C) shows significantly high directivity upto 10.7 dBi and radiation efficiency of 91.59% in both E-plane and H-plane at 1.5 THz. Due to simple structure of proposed antenna, an array implementation could be explored to enhance the radiation parameters. Moreover, the beam steering technique will also be reported for near field scanning of suspicious objects for the detection of hidden explosives in future communication.

References

[1] V. Krozer, T. Löffler, J. Dall, A. Kusk, F. Eichhorn, R.K. Olsson, J.D. Buron, P.U. Jepsen, V. Zhurbenko, T. Jensen, Terahertz imaging systems with aperture synthesis techniques, IEEE Trans. Microw. Theory Tech. 58 (7) (2010) 2027–2039.
[2] C. Hagen, The truth about terahertz, IEEE Spectr. 49 (9) (2012) 36–41.
[3] K.R. Jha, G. Singh, Terahertz planar antennas for future wireless communication: a technical review, Infrared Phys. Technol. 60 (2013) 71–80.
[4] J. Liu, W.-H. Fan, X. Chen, J. Xie, Identification of high explosive RDX using terahertz imaging and spectral fingerprints, Journal of Physics: Conference Series, 680, 1, 2016, pp. 1–9, .
[5] Y. Kurmi, V. Chaurasia, Hidden explosive detection systems for vehicle, Int. J. Comput. Appl. 130 (10) (2015) 16–19.
[6] L.A. Skvortsov, Standoff detection of hidden explosives and cold and fire arms by terahertz time-domain spectroscopy and active spectral imaging (Review), J. Appl. Spectrosc. 81 (5) (2014) 725–749.
[7] E.K. Rahani, T. Kundu, Z. Wu, H. Xin, Mechanical damage detection in polymer tiles by THz radiation, IEEE Sens. J. 11 (8) (2011) 1720–1725.
[8] C. Yu, S. Fan, Y. Sun, E.P. MacPherson, The potential of terahertz imaging for cancer diagnosis: a review of investigations to date, Quant. Imaging Med. Surg. 2 (1) (2012) 33–45.
[9] I. Amenabar, F. Lopez, A. Mendikute, In introductory review to THz non-destructive testing of composite mater, J. Infrared Millim. Terahertz Waves 34 (2) (2013) 152–169.
[10] E.V. Yakovlev, K.I. Zaytsev, I.N. Dolganova, S.O. Yurchenko, Non-destructive evaluation of polymer composite materials at the manufacturing stage using terahertz pulsed spectroscopy, IEEE Trans. Terahertz Sci. Technol. 5 (5) (2015) 810–816.
[11] N. Palka, R. Panowicz, F. Ospald, R. Beigang, 3D non-destructive imaging of punctures in polyethylene composite armor by THz time domain spectroscopy, J. Infrared Millim. Terahertz Waves 36 (8) (2015) 770–788.
[12] K.R. Isha Malhotra, Jha and, G. Singh, Terahertz technology for imaging applications – a technical review, *Infrared Physics and Technology*, (Under Revision), Feb. 2017.
[13] M. Tani, M. Herrmann, K. Sakai, Generation and detection of terahertz pulsed radiation with photoconductive antennas and its application to imaging, Meas. Sci. Technol. 13 (11) (2002) 1739–1745.
[14] H.B. Liu, H. Zhong, N. Karpowicz, Y. Chen, X.C. Zhang, Terahertz spectroscopy and imaging for defense and security applications, Proc. IEEE 95 (8) (2007) 1514–1526.
[15] J. Chen, Y. Chen, H. Zhao, G.J. Bastiaans, X.C. Zhang, Absorption coefficients of selected explosives and related compounds in the range of 0.1–2.8 THz, Opt. Express 15 (19) (2007) 12060–12067.
[16] J.F. Federici, B. Schulkin, F. Huang, D. Gary, R. Barat, F. Oliveira, and David Zimdars, "THz imaging and sensing for security applications-explosives, weapons and drugs", Semicond. Sci. Technol. 20 (2005) S266–S280.
[17] L. Ho, M. Pepper, P. Taday, Terahertz spectroscopy: signatures and fingerprints, Nat. Photon. 2 (2008) 541–543.
[18] A. Grange, Terahertz Spectroscopy: An Investigation into the use of Terahertz Radiation to Detect/sense Drugs, Pharmaceuticals and Polymorphs, Ph.D Thesis, University of Leeds, 2010.
[19] N.M. Burford, M.O. El-Shenawee, Review of terahertz photoconductive antenna technology, Opt. Eng. 56 (1) (2017) 010901/1–01090120.
[20] Yi Huang, N. Khiabani, Y. Shen, D. Li, Terahertz photoconductive antenna efficiency, in: Proc. International Workshop on Antenna Technology (iWAT), Hong Kong, 7–9 March, 2011, pp. 152–156.
[21] D. Saeedkia, Terahertz photoconductive antennas: principles and applications, in: Proceedings of the 5th European Conference on Antennas and Propagation (EUCAP), Rome, Italy, 11–15 April, 2011, pp. 3326–3328.
[22] D.R. Jackson, N.G. Alexopoulos, Microstrip dipoles on electrically thick substrates, Int. J. Infrared Millim. Waves 7 (1) (1986) 1–26.
[23] A.G. Davies, E.H. Linfield, M.B. Johnston, The development of terahertz sources and their applications, Phys. Med. Biol. 47 (2002) 3679–3689.
[24] J.M. Chamberlain, R.E. Miles, C.E. Collins, D.P. Steenson, J.M. Chamberlain, R.E. Miles (Eds.), New Directions in Terahertz Technology, NATO ASI Series, Kluwer, 1997.
[25] M. Tani, Y. Hirota, C.T. Que, S. Tanaka, R. Hattori, M. Yamaguchi, S. Nishizawa, M. Hangyo, Novel terahertz photoconductive antennas, Int. J. Infrared Millim. Waves 27 (4) (2006) 531–546.
[26] T.K. Nguyen, W.T. Kim, B.J. Kang, H.S. Bark, K. Kim, J. Lee, I. Park, T. Jeon, F. Rotermund, Photoconductive dipole antennas for efficient terahertz receivers, Opt. Commun. 383 (2017) 50–56.
[27] N. Zhu, R.W. Ziolkowski, Photoconductive THz antenna designs with high radiation efficiency, high directivity, and high aperture efficiency, IEEE Trans. Terahertz Sci. Technol. 3 (6) (2013) 721–730.
[28] G. Mourou, C.V. Stancampiano, A. Antonetti, A. Orszag, Picosecond microwave pulses generated with a sub-picosecond laser-driven semiconductor switch, Appl. Phys. Lett. 39 (4) (1981) 295–296.
[29] D.H. Auston, K.P. Cheung, P.R. Smith, Picosecond photoconducting hertzian dipoles, Appl. Phys. Lett. 45 (3) (1984) 284–286.
[30] P. Smith, D.H. Auston, M.C. Nuss, Subpicosecond photoconducting dipole antennas, IEEE J. Quantum Electron. 24 (2) (1988) 255–260.
[31] C. Fattinger, D. Grischkowsky, Terahertz beams, Appl. Phys. Lett. 54 (6) (1989) 490–492.
[32] D. Grischkowsky, I.N. Duling III, J.C. Chen, C.C. Chi, Electromagnetic shock waves from transmission lines, Phys. Rev. Lett. 59 (1987) 1663–1666.
[33] J.V. Rudd, M.W.. Warmuth, S.L.. Williamson, D.A.. Zimdars, Compact fiber pigtailed terahertz modules, U.S. Patent 6 816 647, 2004.
[34] C. Fumeaux, G.D. Boreman, W. Herrmann, F.K. Neubuhi, H. Rothuizen, Spatial

impulse response of lithographic infrared antennas, Appl. Phys. Lett. 38 (1999) 37–46.

[35] G.M. Rebeiz, L.F.B. Katehi, W.Y. Ali-Ahmad, G.V. Eleftheriadws, C.C. Ling, Integrated horn antennas for millimetre-wave applications, IEEE Antenna Propag. Mag. 34 (1992) 7–16.

[36] T.K. Nguyen, I. Park, Comparative study of strip-line dipole antenna on semi infinite and lens substrates at terahertz frequency, in: Proceedings of the 8th European Conference on Antennas and Propagation (EuCAP 2014), April 6–11, 2014, Netherlands, pp. 2470–2474.

[37] M. Tani, S. Matsuura, K. Sakai, S.I. Nakashima, Emission characteristics of photoconductive antennas based on low-temperature-grown GaAs and semi-insulating GaAs, Appl. Opt. 36 (30) (1997) 7853–7859.

[38] S. Hughes, M. Tani, K. Sakai, Vector analysis of terahertz transients generated by photoconductive antennas in near-and far-field regimes, J. Appl. Phys. 93 (8) (2003) 4880–4884.

[39] C.W. Berry, M. Jarrahi, Principles of impedance matching in photoconductive antennas, J. Infrared Millim. Terahertz Waves 33 (12) (2012) 1182–1189.

[40] E. Moreno, M.F. Pantoja, F.G. Ruiz, J.B. Roldan, S.G. Garcia, On the numerical modelling of terahertz photoconductive antennas, J. Infrared Millim. Terahertz Waves 35 (5) (2014) 433–444.

[41] J. Yang, W. Fan, B. Xue, Biased electric field analysis of a photoconductive antenna for terahertz generation, Nucl. Instrum. Methods Phys. Res. A 637 (2011) S165–S167.

[42] K.R. Jha, G. Singh, Analysis and design of ring-resonator integrated hemi-elliptical lens antennas at terahertz frequency, Opt. Commun. 285 (16) (2012) 3445–3452.

[43] D. Prather, Millimeter wave imaging using photonic sensors, *Joint Terahertz Imaging System Technology Assessment Workshop*, Falls Church, VA, August 31-September 1, 2005.

[44] N. Khiabani, Y. Huang, Y.-C. Shen, Discussions on the main parameters of THz photoconductive antennas as emitters, in: Proceedings of the 5th European Conference on Antennas and Propagation (EUCAP), 2011, pp. 462–466.

[45] K. Moon, J. Choi, J.H. Shin, S.P. Han, H. Ko, N. Kim, K.H. Park, Generation and detection of terahertz waves using low-temperature-grown GaAs with an annealing process, ETRI J. 36 (1) (2014) 159–162.

[46] T.A. Liu, M. Tani, M. Nakajima, M. Hangyo, K. Sakai, S.I. Nakashima, C.L. Pan, Ultra-broadband terahertz field detection by proton-bombarded InP photocon-ductive antennas, Opt. Express 12 (12) (2004) 2954–2959.

[47] L. Hou, S. Wei, C. Suguo, Noise analysis and optimization of terahertz photo-conductive emitters, IEEE J. Sel. Top. Quantum Electron. 19 (1) (2013) (pp. 8401305-8401305).

[48] M. Venkatesh, K.S. Rao, T.S. Abhilash, S.P. Tewari, A.K. Chaudhary, Optical characterization of GaAs photoconductive antennas for efficient generation and detection of terahertz radiation, Opt. Mater. 36 (2014) 596–601.

[49] S.L. Chuang, Physics of Photonic Devices 80, John Wiley & Sons, 2012.

[50] H.S. Skulason, H.V. Nguyen, A. Guermoune, V. Sridharan, M. Siaj, C. Caloz, T. Szkopek, 110 GHz measurement of large-area graphene integrated in low-loss microwave structures, Appl. Phys. Lett. 99 (15) (2011) (pp. 153504 1-3).

[51] P.Y. Chen, C. Argyropoulos, A. Alu, Terahertz antenna phase shifters using integrally-gated graphene transmission-lines, IEEE Trans. Antenna Propag. 61 (4) (2013) 1528–1537.

[52] M. Dragoman, A.A. Muller, D. Dragoman, F. Coccetti, R. Plana, Terahertz antenna based on graphene, J. Appl. Phys. 107 (2010) 104313/1–104313/3.

[53] I. Llatser, C. Kremers, D.N. Chigrin, J.M. Jornet, M.C. Lemme, A. Cabellos-Aparicio, E. Alarcon, Characterization of graphene-based nano-antennas in the terahertz band, in: Proc. of the 6th IEEE European Conference on Antenna and Propagation (EUCAP), Prague, Czech Republic, March 26–30, 2012, pp. 194–198.

[54] M. Tamagnone, J.S. Gomez-Diaz, J.R. Mosig, J. Perruisseau-Carrier, Analysis and design of terahertz antennas based on plasmonic resonant graphene sheets, J. Appl. Phys. 112 (2012) (pp. 114915/1-4).

[55] F. Miyamaru, Y. Saito, K. Yamamoto, T. Furuya, S. Nishizawa, M. Tani, Dependence of emission of terahertz radiation on geometrical parameters of dipole photo-conductive antennas, Appl. Phys. Lett. 96 (21) (2010) (pp. 211104-1-3).

[56] B. Choudhury, A.R. Sonde, R.M. Jha, Terahertz Antenna Technology for Space Applications, Springer Briefs in Electrical and Computer Engineering, Springer, Singapore, 2016, pp. 1–33.

[57] W.B. Dou, Z.L. Sun, Ray tracing on extended hemispherical and elliptical silicon dielectric lenses, Int. J. Infrared Millim. Waves 16 (11) (1995) 1993–2002.

[58] A.A. Artemenko, A.A. Mal'tsev, R.O. Maslennikov, A.G. Sevastyanov, V.N. Sorin, Studying integrated silicon-lens antennas for radio communication systems operated in the 60 GHz frequency band, Radiophys. Quantum Electron. 55 (8) (2013) 511–519.

[59] Lens antenna with electronic beam steering capabilities, Patent no. WO 2014011087 A1, January 16, 2014.

[60] P.R. Smith, D.H. Auston, M.C. Nuss, Sub-picosecond photoconducting dipole antennas, IEEE J. Quantum Electron. 24 (2) (1988) 255–260.

[61] P.C. Upadhya, W. Fan, A. Burnett, J. Cunningham, A.G. Davies, E.H. Linfield, J. Lloyd-Hughes, E. Castro-Camus, M.B. Johnston, H. Beere, Excitation-density-dependent generation of broadband terahertz radiation in an asymmetrically excited photoconductive antenna, Opt. Lett. 32 (2007) 2297–2299.